Journal of Materials Chemistry B

Accepted Manuscript

ROYAL SOCIETY OF CHEMISTRY

www.rsc.org/materialsB

Reduction Breakable Cholesteryl Pullulan Nanoparticles for Targeted Hepatocellular Carcinoma Chemotherapy

Huanan Li, e-mail: lihuanan1027@163.com

Yani Cui, e-mail:yani0422@126.com

Jun Liu, e-mail:liuxcvr@gmail.com

Shaoquan Bian, e-mail: panda_1987@yahoo.cn

Jie Liang, e-mail: jie_L88@126.com

Yujiang Fan*, e-mail: fan_yujiang@scu.edu.cn

Xingdong Zhang, e-mail: zhangxd@scu.edu.cn

National Engineering Research Center for Biomaterials, Sichuan University,

29 Wangjiang Road, Chengdu 610064, China

*Corresponding authors to whom correspondences and proofs should be sent.

Yujiang Fan

Room 706, Biomaterials Building, Sichuan University,

Chengdu 610064, China

Tel: +86-28-85416196

Fax: +86-28-85410246

E-mail: fan_yujiang@scu.edu.cn

Abstract

In this study, a novel nanoparticular drug delivery platform with inherent targeting ability to hepatic carcinoma cells and reduction triggered drug release property was developed based on reducible cholesterol-modified pullulan (rCHP). Their characteristics and antitumor effects were investigated in vitro and in vivo. The results revealed that drug loaded rCHP nanoparticles were spherical and their diameter ranged between 80-160 nm with the change of molecular structure and drug loading content. rCHP nanoparticles with pullulan shell could anchor to human hepatocellular carcinoma cells (HepG2) due to specific recognition of asialoglycoprotein receptors (ASGPR) overexpressing at the cytomembrane, reduction-sensitively release DOX in tumor cells, and effectively suppress the growth of HepG2 in vitro. In hepatoma-bearing nude mouse model, attributed to their uncharged pullulan surface layer, the nanoparticles efficiently accumulated in tumor site and were internalized by tumor cells. After cellular uptake, DOX release triggered by the reductive circumstance of tumor cells was achieved profited from the reduction-sensitive DOX release property. These nanoparticles showed significantly better antitumor effect and biosafety than DOX·HCl in the nude mice bearing hepatocellular carcinoma tumor.

Key words: Hepatic targeting, reduction-sensitive, pullulan, multifunctional nanoparticle, doxorubicin.

1. Introduction

Multifunctional nanoparticular-drug formulations that specifically recognize cancerous cells and respond to cancerous environment have shown great potential in cancer chemotherapy [1-3]. It has been demonstrated that these multifunctional nanocarriers could accumulate in tumor tissues via enhanced permeability and retention (EPR) effect, effectively enter cancer cells via active targeting (e.g., receptor-mediated endocytosis), and achieve intracellular drug release by the specific cancerous triggers [4-7]. A common strategy for designing the multifunctional nanocarriers is to decorate the surface of nanocarriers with proper ligands that are capable of binding endocytosis-prone receptors expressed at the cancer cells [8, 9]. However, during the process from the injection site to the tumor site through the blood circle, the bioactive surface ligands might increase the probability of nanoparticles captured by reticuloendothelial system (RES) and non-specific attacked by macrophage, and thus decrease the tumor accumulation of the nanocarriers. Recently, arduous efforts have been made in order to settle the above stated issue [10-14]. More sophisticated multifunctional nanoparticles, which could protect the nanoparticles from the capture of reticuloendothelial system (RES) and non-specific attack of macrophage, and expose the ligands to cancer cells after accumulated in tumor site, have been designed and manufactured, for example, with detachable PEG protective layer [15].

Polysaccharides provided the crucial source materials for multifunctional nanoparticular carriers due to their biocompatibility, biodegradability, and autologous cell surface recognition sites [16-18]. Pullulan, a bacterial polysaccharide, has been revealed in many studies as an ideal class of material for development of hepatic targeting drug carriers. Its usefulness in hepatic targeting lies in that it possesses both high blood compatibility and in-built targeting ability to hepatoma carcinoma cells as asialoglycoprotein receptors (ASGPR) ligand [19-23]. Thus nanoparticles derived from pullulan achieve long-term stability in different protein solutions and blood serum. Gd-DTPA-Pullulan and PES-DOX-Pullulan bearing pullulan as ASGPR ligand were

confirmed to provide long circulating property and enhanced targeting to hepatocytes [24, 25]. Cationic pullulan (CP) derivatives can keep stable in plasma and evade immune system. The uptake of CP by HepG2 cells and the liver binding affinity in vivo were significantly enhanced [26].

Controllable release of the cargo drug inside the tumor cells is another crucial aspect for nanocarriers to improve the therapeutic effect of the delivery system. The reduction of disulfide bonds by glutathione has been utilized to design intracellular drug, protein, and gene delivery systems [14, 27] because glutathione in the cytoplasm and cell nucleus is about 100-1000 times higher than that in the circulation [28-31]. Reduction-sensitive nanocarriers containing disulfide bonds respond to the intracellular reductive environment and rapidly release the drug. For instance, He et al. reported that DNA/PEI/HA-SS-COOH had higher gene transfection efficiency for targeted gene delivery [32]. Hubbell et al. reported that PEG-SS-poly(propylene sulfide) delivered and released calcein to cells within 10 min [33]. Sun et al. reported that disulfide bond containing PAA-g-PEG/DOX nanoparticles efficiently deliver doxorubicin into the nuclei of cancer cells [34]. Disulfide cross-linked micelles have also been used to encapsulate DOX for cancer therapy [35, 36].

We report in this study the preparation of doxorubicin (DOX) encapsulated multifunctional nanoparticles with inherent targeting ability to hepatic carcinoma cells and reduction triggered drug release property by coupling cholesterol to pullulan via disulfide bond. Cholesterol, a small endogenous molecule of body's metabolic process, is an optimal choice of hydrophobic groups for preparation of stable self-assembled nanoparticles. Akiyoshi and coworkers successfully prepared pullulan nanogels by partially modifing pullulan with cholesterol groups via an alkyl chain spacer using 1, 6-hexyl diisocyanate [37]. The cholesterol-modified pullulan (CHP) conjugates were reported to be effective to form monodispersed nanoparticles [38-42]. We developed a new method to synthesize the reducible CHP (rCHP) nanoparticles using 3, 3'-Dithiodipropionic acid to replace insensitive exogenous 1, 6-hexyl diisocyanate. We investigated the optimal drug-loading content and drug-release profile of rCHP nanoparticles in vitro. The targeting and penetrating efficiencies of the DOX

encapsulated rCHP nanoparticles were systematically evaluated in vitro and in vivo.

2. Materials and methods

2.1 Materials

Pullulan (MW 0.2 MDa) was purchased from Hayashibara Biochemical Laboratory (Okayama, Japan). Cholesterol, 3, 3'-Dithiodipropionic acid (DTDPA), 1-ethyl-3-[3-(dimethylamino) propyl] carbodiimide hydrochloride (EDC·HCl), N,N′-Dicyclohexylcarbodiimide (DCC), and 4-Dimethylaminopyridine (DMAP) were purchased from Sigma-Aldrich Co. (MO, USA). Doxorubicin hydrochloride (DOX·HCl, >99%) was obtained from Beijing Zhongshuo Pharmaceutical Technology Development Co. (Beijing, China). All other chemicals are of the analytic grade and used as-received.

Human hepatocellular carcinoma cells (HepG2), mouse fibroblast cells (L929) were obtained from Shanghai Institutes for Biological Sciences (China). Balb/c nude mice (4 weeks old, 20–30g) were provided by the Laboratory Animal Center, Sichuan University, China. All handling of animals was performed with the approval of the Institutional Authority for Laboratory Animal Care, Sichuan University.

2.2 Synthesis of reducible cholesterol-modified pullulan (rCHP)

DTDPA (8.41g, 40 mmol), cholesterol (1.93g, 5 mmol) and DMAP (0.0386g, 0.316 mmol) were dissolved in 20 mL anhydrous THF under argon. Then, DCC (3.09 g, 15 mmol) in THF (5 mL) was added dropwise on an ice bath. The formed mixture was stirred at room temperature for 16 h. The reactant was filtrated, the solvents were removed by rotary evaporation, and the product was purified by recrystallization in acetic ether and n-hexane to give cholesterol-dithiodipropionic acid monoester (CDE). ^{1}H-NMR (600 MHz, DMSO): 0.65 (3H, s, cholesterol 18-H3), 0.8-2.4 (28H, cholesterol l-H2, 2-H2, 4-H2, 7-H2, 8-H1, 9-H1, 11-H2, 12-H2, 14-H1, 15-H2, 16-H2, 17-H1, 20-H1, 22-H2, 23-H2, 24-H2 and 25-H1), 0.84 (6H, d, cholesterol 26-H3 and 27-H3), 0.89 (3H, d, cholesterol 21-H3), 0.97 (3H, s, cholesterol 19-H3), 2.60 (4H, m, a-H2), 2.68 (4H, m, b-H2), 4.49 (lH, m, cholesterol 3-H1), 5.35 (lH, m, cholesterol 6-H1).

CDE in dried DMSO was activated by adding EDC (1.5 equivalent CDE) and DMAP (1/100 equivalent CDE). Different amounts of activated CDE (0.05-0.30 equivalent pullulan) were added into 15 mL DMSO solution containing pullulan (0.81 g, 5 mmol). The mixture was stirred at 40°C for 16 h. Then the reactant mixture was dropped into ethanol, the precipitate was collected by centrifugation and washed with anhydrous ethanol, THF, and ethyl acetate, sequentially. Finally the sample was dried under vacuum to obtain rCHP conjugates. The chemical structure of rCHP was confirmed using FT-IR (KBr pellets) and ^{1}H-NMR (DMSO-d6).

2.3 Preparation and characterization of rCHP nanoparticles and DOX-incorporated rCHP (rCHP/DOX) nanoparticles

For preparing rCHP nanoparticles, conjugate was dissolved in DMSO and dropped into deionized water. The solution was transferred into a dialysis membrane tube (Spectra/Por, MWCO 8000-12,000) and dialyzed against deionized water for 24 h with frequent change of water. Then, the product was obtained by freeze-drying.

For preparing DOX-incorporated rCHP (rCHP/DOX) nanoparticles, DOX·HCl was firstly stirred with excess triethylamine (3 equiv DOX·HCl) in DMSO overnight, extracted with $CHCl_3$, and rotary evaporated to obtain DOX base. rCHP (10 mg) was dissolved in 1 ml of DMSO with DOX base (a certain amount), and stirred for 1 h. The solution was dropped into 15 mL deionized water, transferred to a dialysis membrane tube (Spectra/Por, MWCO 8000-12,000) and dialyzed against deionized water at 4 °C for 24 h. The product in the dialysis tube was obtained subsequently by freeze-drying. The amount of incorporated DOX was measured by UV absorbance at 485 nm in DMSO. Loading capacity (LC) and encapsulation efficiency (EE) were calculated by the following equations.

LC (wt%) = [weight of loaded drug/weight of drug loaded nanoparticles]×100%

LE (%) = [weight of loaded drug/weight of drug in feed] ×100%

The size distribution, zeta potential and morphology of the nanoparticles were characterized using dynamic light scattering (DLS, Malvern Nano-ZS) and transmission electronic microscopy (TEM, Hitachi H-600).

2.4 In vitro drug release of rCHP/DOX nanoparticles

The release profiles of rCHP/DOX nanoparticles were studied using a dialysis tube (MWCO 8000-12,000) at 37°C in PBS buffer (100 mM, pH 7.4) with 10 mM DTT or without DDT. Drug release studies were performed by dialyzing 1.0 mL of nanoparticle solution (nanoparticle concentration 1mg/mL) against 25 mL of the same medium (MWCO 8000-12,000). At certain time intervals, 1.0 mL of release media was taken out and replenished with an equal volume of fresh media. The amount of released DOX was determined using fluorescence measurement (F-7000, excitation at 485 nm). The release experiments were conducted in triplicate and the results presented were the average data with standard deviations.

For monitoring the size change of rCHP/DOX nanoparticles under the reduction condition, 1 mg rCHP/DOX nanoparticle was dissolved in 1mL PBS containing 10 mM DTT. At certain time interval, the size of nanoparticle was monitored by DLS measurement.

2.5 Cell culture

L929 cells (mouse fibroblast cells) and HepG2 cells (human liver cancer cells) were cultured in Dulbecco's Modified Eagle's Medium (DMEM) supplemented with 10% fetal bovine serum, 100 IU/mL penicillin and 100 μg/mL streptomycin at 37 °C in a humidified atmosphere with 5% CO_2.

2.6 Cellular uptake of rCHP/DOX nanoparticles and intracellular distribution of DOX

Confocal laser scanning microscopy (CLSM) and flow cytometry were employed to examine the cellular uptake and intracellular distribution of DOX for rCHP/DOX nanoparticles and DOX·HCl. Briefly, cell lines (HepG2 and L929) were cultured for 1 day in 24-well cell culture plate (2×10^4 cells/well). Then the culture media was replaced with 1 mL media containing nanoparticles or DOX·HCl (DOX content: 5 mg/L). After 2, 4, 8, and 12 h culture, respectively, the culture media was removed and the cells were rinsed twice with PBS to remove nanoparticles or DOX·HCl which were not ingested by the cells. Then the cell nuclei were stained with DAPI. The cells were observed with CLSM (Leica TCP SP5, Germany). DOX was excited at 485 nm with the emission at 595 nm.

The quantitative cellular uptake of rCHP/DOX nanoparticles and DOX·HCl was further evaluated in HepG2 cells via flow cytometry. The cells were seeded onto

6-well plate at a density of 3×10^5 cells/well, and maintained for 24 h at 37°C, 5% CO_2. The cells were then treated with rCHP/DOX nanoparticles (1mg/L equivalent DOX concentration) and DOX·HCl (1mg/L) for 1, 2, 4 and 8 h. The cells were then washed comprehensively with PBS, trypsinized and collected by centrifugation at 1000 rpm for 5 min. The cell pellet was re-suspended in PBS (0.5mL) and assessed for fluorescent intensity per cell and percentage of cells that internalized DOX. Auto-fluorescence produced by the cells was taken into account by referencing the fluorescent intensity measurement of the treated cell sample to that given by HepG2 cells without any treatment. The measurements were done with excitation and emission wavelengths of 532 and 595 nm respectively.

2.7 In vitro cellular growth inhibition of rCHP/DOX nanoparticles

Growth inhibition effect of rCHP/DOX nanoparticles and free DOX·HCl (for compare) was evaluated by the standard methylthiazoltetrazolium (MTT) assay as described previously [43]. L929 and HepG2 cells harvested in logarithmic growth phase were seeded onto 96-well plates at a density of 4×10^3 cells/well and left overnight in the incubator. rCHP/DOX nanoparticles or DOX·HCl were dissolved in the cell culture medium at various concentrations. 100μL of the media, in which the DOX concentrations were 0.0001, 0.001, 0.01, 0.1, 1.0, and 10.0 mg/L, respectively, were used to substitute the media in each well. The cells were incubated for 48 h before being assayed for viability via MTT assay.

2.8 In vivo and ex vivo bio-distribution

Balb/c nude mice (4 weeks old, 20-30 g) were injected subcutaneously in the back with 0.1 mL of a cell suspension containing HepG2 cells (4×10^6 cells/animal). When the tumor volume reached approximately 70-100 mm^3, rCHP/DOX nanoparticles, DOX·HCl, and PBS were injected via tail vein at a dosage of DOX (10 mg/kg). The mice were then anesthetized and imaged by an in vivo imaging system (Maestro Ex Pro, CRI, USA) with a 12-bit CCD camera equipped with a near infrared emission filter (500-950 nm) from 2h to 8h. After each imaging point, the mouse was euthanized by over anesthesia and tumor was excised and frozen rapidly in dry ice, allowing the generation of 10 μm thick cryosections. The tissue sections were fixed in cold acetone for 10 min, washed with PBS, and stained with the DAPI (Sigma). Images were captured using CLSM (Leica TCP SP5, Germany).

2.9 In vivo antitumor effect of rCHP/DOX nanoparticles in hepatocellular carcinoma subcutaneous model

The mice bearing tumors were divided into eight groups (n = 9). DOX·HCl, and rCHP/DOX nanoparticles were suspended in PBS to prepare the drug solutions (equivalent DOX concentration 100 μg/mL). Blank rCHP 3 nanoparticle solution was prepared with concentration corresponding to the rCHP 3 in rCHP 3a nanoparticle solution. Then physiological saline (control), rCHP 3 nanoparticle, DOX·HCl, and rCHP/DOX nanoparticles (equivalent dose of DOX = 5mg/kg bodyweight) solutions were injected through tail veins for 5 times at a 3 day interval. Because the nanoparticles formulations of DOX are much more tolerated as we researched previously, the rCHP/DOX nanoparticles were also administered at higher dose (20 mg/kg, 40 mg/kg) to determine if the anti-tumor effect could be enhanced.

Tumor volumes and body weight were measured for 25 days. The tumor volume was calculated as follows:

$$\text{Tumor volume } (mm^3) = width^2 \times length/2.$$

After 25 days, 3 mice in each group were euthanized. The heart, liver, spleen, lung, kidney, and tumor were separated and weighted, and then washed with PBS and fixed in 10% formaldehyde for 24 h for histological examination. The histological slices obtained were stained with haematoxylin/eosin (H&E) and observed by optical microscopy. For humanistic reasons, other animals were euthanized when the implanted tumor volume reached 1000 mm^3, which was considered as the end point of survival data.

2.10 Statistical analysis

The results are presented as the mean value with standard deviation (mean±SD). Statistical analysis was performed using two-tailed, unpaired t-tests between data sets. Probability values less than 0.05 ($p<0.05$) were considered to indicate a statistically significant result.

3. Results and discussion

3.1 Synthesis and characterization of rCHP

Due to the flexibility in their structural modifications, polysaccharides could

expediently react with various molecules to fulfill different demands. Therefore, polysaccharides have gained increasing attention for specific biomedical applications. In this work, a new reducible CHP (rCHP) conjugate was constructed according to Scheme 1. To attach hydrophobic cholesterol to water soluble pullulan, cholesterol was at first reacted with 3, 3'-dithiodipropionic acid to obtain cholesterol-dithiodipropionic acid monoester (CDE). Then, the carboxyl of CDE was activated using EDC with DMAP as the catalyst, and coupled to pullulan. The final product was easily purified by dialysis against water and freeze-drying, and the structure was confirmed employing FT-IR and ^{1}H-NMR as illustrated in Fig. 1 for the representative spectra of rCHP 1. The FT-IR spectrum of rCHP exhibited the characteristic absorption band at 1724 cm^{-1} due to the carbonyl group stretching vibration. According to previous assignment made by Akiyoshi and Yang [37, 44], rCHP ^{1}H-NMR spectrum permitted the identification of the protons: 2.60 ppm (4H, m, a-H2), 2.68 ppm (4H, m, b-H2), 3.00-4.00 ppm (4H, glucose C2, C3, C4, and C5), 4.60-5.40 ppm (glucose, -OH), 4.67 ppm (1H, s, 1-glueose α-1,6), 5.03 ppm (1H, s, 2-glueose α-1,4). The degree of substitute (number of cholesterol residues per 100 glucose unites in pullulan) could be determined by the ratio of methylene groups protons (2.60 ppm) to sugar protons (C1 position of α-1,6 and α-1,4 glycosidic bonds, 4.67 and 5.03 ppm) [45]. By controlling the feed ratio of CDE to pullulan during the synthesis procedure, conjugates with DS 3.6-8.3 could be obtained (Table 1). It has been reported that cholesterol modified pullulan with these DS were benefited to form nanoparticles having good monodispersity [38].

rCHP self-assembled in water to form nanoparticles with diameter ranging from 57.4-89.1 nm and narrow size distributions (PDI less than 0.2) depending on the DS value (Table 1). Interestingly, when the DS of rCHP increased from 3.6 to 6.3, the size of nanoparticles decreased from 74.3 nm to 57.4 nm. Whereas when DS further increased, size of nanoparticles also increased. This phenomenon was explained that at low DS, the increase of DS enhanced the hydrophobic interaction among cholesterol molecules and resulted in the formation of more compact and stable hydrophobic cores. Further increase of the cholesterol in the conjugate might result in the aggregation of more conjugates through hydrophobic segment interaction and thus

increase the size.

The self-assembled nanoparticles possessed good stability. After being lyophilized to dry powder and simply dispersed in water again, the formed nanoparticles showed the same mean diameter and narrow size distribution. The thus formed nanoparticles kept unchanged up to 6 months. The zeta potentials of rCHP nanoparticles were near zero in aqueous media because of nonionic nature of pullulan. Previous studies have showed that the nanoparticles with positively charge were cleared rapidly from the circulation after administration, whereas the uncharged and negatively charged nanoparticles could prevent the strong interaction with serum proteins and macrophage uptake in the circulation system [46].

3.2 Drug loading and reduction triggered drug release of rCHP/DOX nanoparticles

DOX was encapsulated in the nanoparticles by dialyzing the DMSO solution of rCHP and DOX against water. The formed rCHP/DOX nanoparticles were spherical in shape, mono-distributed in size and homogeneous (Fig. 2). DOX-loading capacities were affected by the properties of rCHPs (Table 2). Generally, rCHP with higher DS had higher drug loading content (DLC) and higher drug encapsulation efficiency (EE). With the same drug/rCHP ratio of 10/100 (w/w), the DLC increased from 6.08% for rCHP 1a to 8.77% for rCHP 3a, and the EE also increased from 66.79% to 96.37%, respectively. To investigate the drug loading capacity of the nanoparticles, we choose rCHP 3, which formed non-loading nanoparticles with the smallest size, for further study. When the drug/rCHP ratio increased from 10/100 to 50/100 (w/w), the DLC increased from 8.77% (rCHP 3a) to 27.75% (rCHP 3d), but the EE decreased from 96.37% to 83.27%. Meanwhile, the size also increased from 91.7 nm to 157.8 nm. It has been reported that nanoparticles with diameter less than 150 nm and favorable monodispersity were considered to contribute to extravasation into tumors through EPR effect but also small enough to escape capture by fixed macrophages that are lodged in the reticuloendothelial system, such as the spleen and liver, while those smaller than 20 nm have been reported to be excreted through renal clearance, which will also decrease the longevity of the NPs after injection *in vivo* [47-52]. Thus these rCHP/DOX nanoparticles with diameter 80-160 nm could benefit the delivery of

drugs into tumor.

In vitro drug release studies were performed under reducing conditions that mimic the intracellular environment of cancer cells using DTT as the reduction agent at pH 7.4 and 37 °C. The representative release profiles for rCHP 1a (DLC 6.08%), rCHP 3a (DLC 8.77%) and rCHP 3c (DLC 26.35%) nanoparticles were shown in Fig. 3A. Without the existence of DTT, only small amount of drug (less than 10%) was released from all these nanoparticles within the first 12 h. Afterwards, there was almost no further release until 24 h. However, drug release was significantly enhanced in the presence of 10 mM DTT under otherwise the same conditions. DOX release from nanoparticles was rapid and about 50-60% of DOX was released within the first 5 h at reductive environment. After 24 h, 93.57%, 88.41%, and 85.27% drug was released from reduction-sensitive rCHP 1a, rCHP 3a, and rCHP 3c nanoparticles, respectively. Meanwhile, under the condition without the existence of DTT, sizes of nanoparticles were rather stable, kept their initial size within the whole releasing period (Fig. 3B). When there was 10 mM DDT in the system, sizes of all the 3 nanoparticles increased at the early period, due to the cleavage of disulfide bond and detachment of cholesterol under reductive condition that decreased the hydrophobic interaction and resulted in the subsequent loose structure of the core. [53] After certain time, the nanoparticles were not detectable, which implied that the remanent cholesterol on the conjugate could no longer provide enough hydrophobic interaction to form the nanoparticles.

Compared with the release behavior of rCHP 3a nanoparticles, the lower DS rCHP 1a nanoparticles showed more release at the same time interval under 10 mM DTT. Also, the breakdown of rCHP 1a nanoparticles was earlier than that of rCHP 3a. This is probably because that release characteristics depended much on hydrophobic/hydrophilic segments ratio. When ratio of hydrophobic segments and hydrophilic segments was close to optimal value, the nanoparticles were compact and stable, and probability of DTT penetrating into hydrophobic core of nanoparticles became lower. Thus collapse of nanoparticles and drug release were slower. It is also worth to notice that rCHP 3c released less drug at the same time interval than rCHP

3a, which had same DS with the former but lower DLC. The breakdown of rCHP 3c was also late compared with rCHP 3a, suggesting that the hydrophobic interaction and π–π stacking between DOX molecules could also contribute to the formation the drug-loaded nanoparticles.

3.3 Cellular uptake of rCHP/DOX nanoparticles and intracellular distribution of DOX

The cellular uptake of rCHP nanoparticles was examined using both flow cytometry and confocal laser scanning microscopy (CLSM). Fig. 4 showed the flow cytometry histograms of HepG2 cells incubated with DOX·HCl and rCHP 3c nanoparticles for 1, 2, 4 and 8 h, respectively. After 1, 2, and 4 h, the florescence strength of DOX in cells incubated with rCHP 3c nanoparticles was stronger than those incubated with DOX·HCl, probably due to the superiority of receptor mediated endocytosis pathway of pullulan nanoparticles over the diffusion mechanism of DOX·HCl [54]. When the incubation time elongated to 8 h, the florescence in cells incubated with rCHP 3c nanoparticles did almost not increase compared with that after 4 h, but the florescence in cells incubated with DOX·HCl increased obviously and became stronger than that with rCHP 3c nanoparticles. In an investigation of nanoparticles effect on MSC cells, Li et al. reported that to each MSC cell, up to 1500 nanoparticles could be internalized [55]. In our case of nanoparticles, with the increase of incubation time, nanoparticles internalized by cells might reach a limit. On the other hand, DOX·HCl might keep diffusing into the cells.

CLSM observation (Fig. 5) revealed the intracellular distribution of DOX in HepG2 cells incubated with rCHP 3c nanoparticles and DOX·HCl. Different from DOX·HCl, when incubated the cells with nanoparticles, a lot of red light pots were observed inside cytoplasm at 2 h, but only very weak florescence in the nucleus was detected. This phenomenon was in accordance with the endocytosis pathway of nanoparticle internalization in which nanoparticles were internalized with the formation of endosomes. After 4 h and 8 h incubation, DOX florescence in nuclei became obvious, indicating that some drug entered nuclei because of the DOX release from nanoparticles due to the high reducing agent (GSH) concentration inside tumor cells.

When the incubation period was elongated to 12 h, DOX fluorescence in cytoplasm became very weak, and most florescence was detected in cells nuclei. In contrast, although DOX·HCl could also be effectively internalized by L929 cells, the uptake of nanoparticles by non-targeted L929 cells was rather weak compared with that in HepG2 cells. These results indicated that rCHP/DOX nanoparticle showed limited internalization of non-targeted L929 cells, but could be specifically recognized and taken up by its target HepG2 cells

3.4 Growth inhibition of rCHP/DOX nanoparticles on HepG2 cells

Specific killing efficiency also investigated by incubating non-targeted cells and targeted cells with rCHP3c nanoparticles. Since rCHP/DOX nanoparticles having pullulan surface layer can bind specifically to ASGPR-abundant HepG2 cells, the inhibition concentration (IC50) of rCHP 3c on HepG2 cells was quite similar to that for DOX·HCl (0.0243 *vs*. 0.0178mg/L). On the other hand, when non-targeted L929 cells without high expression of ASGPR were tested under identical experimental conditions, in contrast to the dramatic cytotoxic effect of rCHP 3c to HepG2 cells, the killing efficacy of rCHP 3c toward L929 cells was significantly less than that of DOX·HCl due to lower cellular uptake amounts. These results were in accordance with our previous report that pullulan nanoparticles enhanced the uptake more effectively in HepG2 cells than in L929 cells [56]. This comparative study further provided strong evidence for the specific recognition and cellular uptake of pullulan nanoparticle by its target HepG2 cells.

3.5 Tumor accumulation of rCHP/DOX nanoparticles

One of the important concerns after intravenous injection of nanoparticle formula is that whether the nanoparticles could accumulate in tumor. The tumor accumulation behavior of rCHP 3c nanoparticles was determined based on the fluorescence optical imaging technique, which is a powerful tool for *in vivo* tracking of drugs transport in nude mice and widely used for evaluating drug targeting to tumor. [57] rCHP 3c and DOX·HCl were administrated into hepatoma tumor-bearing nude mice, and were clearly visualized by monitoring real-time fluorescence intensity in the whole body over the course of 8 h (Fig. 7 A). When the mice were treated with DOX·HCl, DOX

fluorescence was found wildly dispersed in the body with slightly stronger intensity at the tumor site. The intensity increased gradually from 2 h to 4 h after injection. Then the decrease of fluorescence was observed after 8 h. In contrast, in the mice treated with rCHP 3c nanoparticles, the fluorescent signals at the tumor site were much stronger than that at the normal tissues, which revealed a clear discrimination between subcutaneous tumors and the surrounding normal tissue. The fluorescence intensity kept strong in the tumor site over 8 h. This high tumor targeting ability demonstrated that rCHP/DOX nanoparticles might enhance the tumor accumulation of loaded drug and maintain for longer time due to EPR effect of nanoparticles, most likely benefited from the excellent blood compatibility of pullulan which decreased blood clearance and prolonged circulation period of the nanoparticles. [58]

It was very important to confirm that the drugs were not only concentrated in tumor but also internalized by hepatoma carcinoma cell. The tumor was excised from the mice after treated with rCHP 3c nanoparticles, frozen sliced and stained with DAPI to locate the nuclei. CLSM images clearly showed that DOX could be distinguished in the hepatocytes because of the receptor mediated endocytosis that allowed rapid internalization after the nanoparticles accumulated in tumor (Fig. 7 B). After 2 h, red fluorescence for the DOX was found to overlap the blue stained nuclei of the cells. DOX signal was still found between the nuclei position in samples for 2 h and 4 h after injection, suggesting that some drug was still encapsulated in nanoparticles and located in endosome/lysosome in cytoplasm. After 8 h, the red signal of DOX almost completely overlapped with the nuclei blue signal. Only very weak DOX fluorescence was detected between the blue nuclei area. This indicated that the drugs in nanoparticles could be effectively released in the reductive circumstance of tumor cells.

3.6 In vivo antitumor effect of rCHP/DOX nanoparticles

To evaluate antitumor activity and toxicity of rCHP/DOX nanoparticles, nanoparticles and DOX·HCl were intravenously injected into mice bearing hepatoma model at 5 different time points with an interval of 3 days (day 1, 4, 7, 10, and 13). Fig. 8 A showed the tumor growth curves after treatment. The tumors in all

drug-treated groups showed growth retardation compared to the control group injected with PBS. Compared with DOX·HCl, rCHP/DOX nanoparticles exerted more effective antitumor activity over a broad range of injection doses (up to 40 mg/kg equivalent DOX dose) to suppress tumor growth. In the case of DOX·HCl, the mice treated with 15 mg/kg dose were dead within one day due to the toxicity of the drug. This corresponded well to the fact that the DOX·HCl lethal dose killing 50% of the test animals within a designated period is generally 12.7-13.2 mg/kg [59]. On the contrary, rCHP 3c nanoparticles were safely injectable up to a 40mg/kg dose without the death of treated mice, and more effectively depressed the growth of tumor compared with the 5 mg/kg dose of the same nanoparticle formula. At the end of in vivo experiment, the tumors of all groups were removed, photographed and weighted. The sizes of tumors from mice administrated by rCHP/DOX nanoparticles were obviously smaller than those from DOX·HCl treated group and control group (Fig. 8 B), which was proportional to the observed relative tumor volume results. Simultaneously, the weights of tumors in mice treated with nanoparticles were obviously lower compared with the tumors from DOX·HCl treated group and control group ($p < 0.05$) (Fig. 8 B). These results demonstrated the high antitumor activity of rCHP/DOX nanoparticles in hepatocellular carcinoma subcutaneous model in animal experiment, namely, the therapeutic efficacy of rCHP/DOX nanoparticles was significantly improved over that of DOX·HCl that has a narrow therapeutic window between 5 and 10 mg/kg because of its toxicity and adverse side effect.

3.7 Systemic toxicity of rCHP/DOX nanoparticles in nude mice

The potential adverse effect of cancer chemotherapy remains a primary concern for its clinical applications. In the present study, the change of body weight was analyzed as an important indicator for treatment-induced toxicity of different drug formula (Fig. 9 A). On day 25, the nude mice bearing hepatoma treated with PBS (control group) increased their body weights by 31%. The rCHP/DOX nanoparticle treated groups had bodyweights growth between 24-29% even with high dosage. When 5 mg/kg DOX dose was applied, the weight growths were not significantly different from that of control group, indicating that these treatments were well tolerated in nude mice.

When 20 and 40 mg/kg DOX dose were applied, the increase of body weight became mitigatory, and significantly different from that of control group, probably because of the depressed growth of tumor. In contrast, administration of DOX·HCl in the nude mice bearing hepatoma resulted in near 20% weight lost compared with the initial value, despite the notable growth of tumor. Meanwhile, histological analysis of mice treated with PBS and rCHP/DOX nanoparticles revealed no significant signal of damage from H&E stained organ slices including heart, liver, spleen, lung and kidney (Fig. 9 B). However, for DOX·HCl treated group, obvious organ damage of necrosis with acute inflammatory cells infiltration were perceived in heart and kidney tissues compared with the muscle fibers and organ structure from control mice. As a result, compared with DOX·HCl, rCHP/DOX nanoparticles obviously elongated the life span of hepatoma tumor-bearing nude mice, especially when high equivalent DOX dosages were applied (Fig. 9 C). These findings indicated that encapsulation of DOX in the nanoparticles greatly decreased the toxicity and adverse side effect of DOX while effectively enhanced its anticancer activity.

4. Conclusion

A series of DOX-loaded reducible cholesterol graft pullulan (rCHP) nanoparticles were prepared. Their characteristics and antitumor effects were investigated. The results revealed that these nanoparticles were less than 200 nm in diameter with high drug loading content. Drug released from nanoparticles in a reduction-sensitive manner, and effectively inhibited the growth of HepG2 in vitro. Attributed to their uncharged pullulan surface layer and reduction-triggered DOX release property, these nanoparticles showed remarkable antitumor effect in the nude mice bearing hepatocellular carcinoma tumors, most likely through the increased accumulation in tumor, enhanced internalization by receptor mediated endocytosis, and accelerated DOX release in tumor cells.

Acknowledgment

This work was sponsored by National Natural Science Foundation of China (grant No. 21174090). The authors thank Mr. Xiaoli Zhu for his help in animal experiments.

References

1 K. S. Soppimath, L. H. Liu, W. Y. Seow, S. Q. Liu, R. Powell, P. Chan and Y. Y. Yang, *Adv. Funct. Mater.*, 2007, **17**, 355-362.

2 Y. Yan, A. P. Johnston, S. J. Dodds, M. M. Kamphuis, C. Ferguson, R. G. Parton, E. C. Nice, J. K. Heath and F. Caruso, *ACS Nano*, 2010, **4**, 2928-2936.

3 L. Brannon-Peppas and J. O. Blanchette, *Adv. Drug Delivery. Rev.*, 2012, **64**, 202-216.

4 R. Li, R. a. Wu, L. Zhao, M. Wu, L. Yang and H. Zou, *ACS Nano*, 2010, **4**, 1399-1408.

5 P. Xu, E. A. Van Kirk, Y. Zhan, W. J. Murdoch, M. Radosz and Y. Shen, *Angew. Chem., Int. Ed.*, 2007, **46**, 4999-5002.

6 F. Lacoeuille, E. Garcion, J.-P. Benoit and A. Lamprecht, *J. Nanosci. Nanotechnol.*, 2007, **7**, 4612-4617.

7 C. Vauthier, C. Dubernet, C. Chauvierre, I. Brigger and P. Couvreur, *J. Control. Release*, 2003, **93**, 151-160.

8 M. D. Wang, D. M. Shin, J. W. Simons and S. Nie, *Expert Rev. Anticancer Ther.*, 2007, **7**, 833-837.

9 T. M. Allen, *Nat. Rev. Cancer*, 2002, **2**, 750-763.

10 F. Zhang, G. B. Braun, A. Pallaoro, Y. Zhang, Y. Shi, D. Cui, M. Moskovits, D. Zhao and G. D. Stucky, *Nano Lett.*, 2011, **12**, 61-67.

11 Y.-L. Luo, Y.-S. Shiao and Y.-F. Huang, *ACS Nano*, 2011, **5**, 7796-7804.

12 Y.-X. Zhao, A. Shaw, X. Zeng, E. Benson, A. M. Nyström and B. r. Högberg, *ACS Nano*, 2012, **6**, 8684-8691.

13 M. Gingras, J. M. Raimundo and Y. M. Chabre, *Angewandte Chemie International Edition*, 2007, **46**, 1010-1017.

14 R. E. Wang, F. Costanza, Y. Niu, H. Wu, Y. Hu, W. Hang, Y. Sun and J. Cai, *J. Control. Release*, 2012, **159**, 154-163.

15 S. Zhu, M. Niu, H. O'Mary and Z. Cui, *Mol Pharm*, 2013, **10**, 3525-3530.

16 Y.-Z. Du, Q. Weng, H. Yuan and F.-Q. Hu, *ACS Nano*, 2010, **4**, 6894-6902.

17 Z. Liu, Y. Jiao, Y. Wang, C. Zhou and Z. Zhang, *Adv. Drug Delivery. Rev.*, 2008, **60**, 1650-1662.

18 S. Mao, W. Sun and T. Kissel, *Adv. Drug Delivery. Rev.*, 2010, **62**, 12-27.

19 M. Rekha and C. P. Sharma, *Trends Biomater Artif Organs*, 2007, **20**, 116-121.

20 D. Trerè, L. Fiume, L. B. De Giorgi, G. Di Stefano, M. Migaldi and M. Derenzini, *Br. J. Cancer*, 1999, **81**, 404.

21 T. Yamaoka, Y. Tabata and Y. Ikada, *Drug Delivery*, 1993, **1**, 75-82.

22 S. Yuen, *Process Biochemistry*, 1974, **9**.

23 Y. Kaneo, T. Tanaka, T. Nakano and Y. Yamaguchi, *J. Control. Release*, 2001, **70**, 365-373.

24 S. A. Guhagarkar, R. V. Gaikwad, A. Samad, V. C. Malshe and P. V. Devarajan, *Int. J. Pharm.*, 2010, **401**, 113-122.

25 H. Yim, S. G. Yang, Y. S. Jeon, I. S. Park, M. Kim, D. H. Lee, Y. H. Bae and K. Na, *Biomaterials*, 2011, **32**, 5187-5194.

26 M. R. Rekha and C. P. Sharma, *Biomaterials*, 2009, **30**, 6655-6664.

27 Y. Li, K. Xiao, J. Luo, W. Xiao, J. S. Lee, A. M. Gonik, J. Kato, T. A. Dong and K. S. Lam, *Biomaterials*, 2011, **32**, 6633-6645.

28 F. Meng, W. E. Hennink and Z. Zhong, *Biomaterials*, 2009, **30**, 2180-2198.

29 R. Cheng, F. Feng, F. Meng, C. Deng, J. Feijen and Z. Zhong, *J. Control. Release*, 2011, **152**, 2-12.

30 G. Saito, J. A. Swanson and K.-D. Lee, *Adv. Drug Delivery. Rev.*, 2003, **55**, 199-215.

31 R. Wei, L. Cheng, M. Zheng, R. Cheng, F. Meng, C. Deng and Z. Zhong, *Biomacromolecules*, 2012, **13**, 2429-2438.

32 Y. He, G. Cheng, L. Xie, Y. Nie, B. He and Z. Gu, *Biomaterials*, 2013, **34**, 1235-1245.

33 S. Cerritelli, D. Velluto and J. A. Hubbell, *Biomacromolecules*, 2007, **8**, 1966-1972.

34 Y. Sun, W. Zou, S. Bian, Y. Huang, Y. Tan, J. Liang, Y. Fan and X. Zhang, *Biomaterials*, 2013, **34**, 6818-6828.

35 A. N. Koo, H. J. Lee, S. E. Kim, J. H. Chang, C. Park, C. Kim, J. H. Park and S. C. Lee, *Chem. Commun.*, 2008, **48**, 6570-6572.

36 Y. L. Li, L. Zhu, Z. Liu, R. Cheng, F. Meng, J. H. Cui, S. J. Ji and Z. Zhong, *Angewandte Chemie International Edition*, 2009, **48**, 9914-9918.

37 K. Akiyoshi, S. Deguchi, N. Moriguchi, S. Yamaguchi and J. Sunamoto, *Macromolecules*, 1993, **26**, 3062-3068.

38 W.-z. Yang, H.-l. Chen, F.-p. Gao, M.-m. Chen, X.-m. Li, M.-m. Zhang, Q.-q. Zhang, L.-r. Liu, Q. Jiang and Y.-s. Wang, *Current Nanoscience*, 2010, **6**, 298-306.

39 K. Akiyoshi, S. Kobayashi, S. Shichibe, D. Mix, M. Baudys, S. Wan Kim and J. Sunamoto, *J. Control. Release*, 1998, **54**, 313-320.

40 Y. Ikuta, N. Katayama, L. Wang, T. Okugawa, Y. Takahashi, M. Schmitt, X. Gu, M. Watanabe, K. Akiyoshi and H. Nakamura, *Blood*, 2002, **99**, 3717-3724.

41 K. Satoh, F. Chen, A. Aoyama, H. Date and K. Akiyoshi, *European Journal of Cancer Supplements*, 2008, **6**, 139.

42 J. Sunamoto, K. Ushio and D. T. Lai, *J. Bioact. Compat. Polym.*, 2006, **21**, 603-617.

43 M. B. Hansen, S. E. Nielsen and K. Berg, *J Immunol Methods*, 1989, **119**, 203-210.

44 W. Yang, M. Wang, L. Ma, H. Li and L. Huang, *Carbohydrate polymers*, 2014, **99**, 720-727.

45 P. Sivakumar and K. Panduranga Rao, *Carbohydrate polymers*, 2003, **51**, 327-332.

46 F. Alexis, E. Pridgen, L. K. Molnar and O. C. Farokhzad, *Mol Pharm*, 2008, **5**, 505-515.

47 Y. C. Chen, L. C. Liao, P. L. Lu, C. L. Lo, H. C. Tsai, C. Y. Huang, K. C. Wei, T. C. Yen and G. H. Hsiue, *Biomaterials*, 2012, **33**, 4576-4588.

48 K. F. Pirollo and E. H. Chang, *Trends Biotechnol*, 2008, **26**, 552-558.

49 W. Jiang, B. Y. Kim, J. T. Rutka and W. C. Chan, *Nat. Nanotechnol*, 2008, **3**, 145-150.

50 M. E. Davis, Z. G. Chen and D. M. Shin, *Nat. Rev. Drug Discov.*, 2008, **7**, 771-782.

51 H. S. Choi, W. Liu, P. Misra, E. Tanaka, J. P. Zimmer, B. Itty Ipe, M. G. Bawendi and J. V. Frangioni, *Nat Biotechnol*, 2007, **25**, 1165-1170.

52 O. Veiseh, J. W. Gunn and M. Zhang, *Adv Drug Deliv Rev*, 2010, **62**, 284-304.

53 W. W. Gao, R. Langer and O. C. Farokhzad, *Angew. Chem., Int. Ed.*, 2010, 49, 6567–6571

54 L. Jiang, X. Li, L. Liu and Q. Zhang, *International journal of nanomedicine*, 2013, **8**, 1825-1834.

55 L. Li, Y. Guan, H. Liu, N. Hao, T. Liu, X. Meng, C. Fu, Y. Li, Q. Qu, Y. Zhang, S. Ji, L. Chen, D. Chen and F. Tang, *ACS Nano*, 2011, **5**, 7462-7470.

56 H. Li, S. Bian, Y. Huang, J. Liang, Y. Fan and X. Zhang, *J Biomed Mater Res A*, 2013, **102**, 150-159.

57 S. Jiang, M. K. Gnanasammandhan, and Y. Zhang. *J. Roy. Soc. Interface*, 2010, **7**, 3-18.

58 D. Lu, J. Liang,Y. Fan, Z. Gu and X. Zhang, *Adv. Eng. Mat.*, 2010, **12**, B496-B503.

59 P. M. Kanter, G. A. Bullard, F. G. Pilkiewicz, L. D. Mayer, P. R. Cullis and Z. P. Pavelic, *In Vivo*, 1993, **7**, 85-95.

Table 1 Characteristic of rCHP self-assembled nanoparticle

Sample	Pullulan/CDE(mol/mol)	DS(%)	diameter(nm)	PDI
rCHP **1**	100/5	3.6	74.3	0.134
rCHP **2**	100/7.5	5.2	69.7	0.191
rCHP **3**	100/10	6.3	57.4	0.147
rCHP **4**	100/12.5	7.9	76.4	0.126
rCHP **5**	100/15	8.3	89.1	0.185

Table 2 Characteristic of DOX-loaded rCHP(rCHP/DOX) nanoparticle

Sample	Feed ratio	Obtained nanoparticles			
	DOX:CHSP(w/w)	DLC(%)	EE(%)	diameter(nm)	PDI
rCHP **1a**	10:100	6.08	66.79	82.1	0.171
rCHP **2a**	10:100	7.44	81.85	87.8	0.109
rCHP **3a**	10:100	8.77	96.37	91.7	0.183
rCHP **3b**	15:100	12.08	92.65	97.4	0.128
rCHP **3c**	40:100	26.35	92.21	139.2	0.172
rCHP **3d**	50:100	27.75	83.27	157.8	0.112

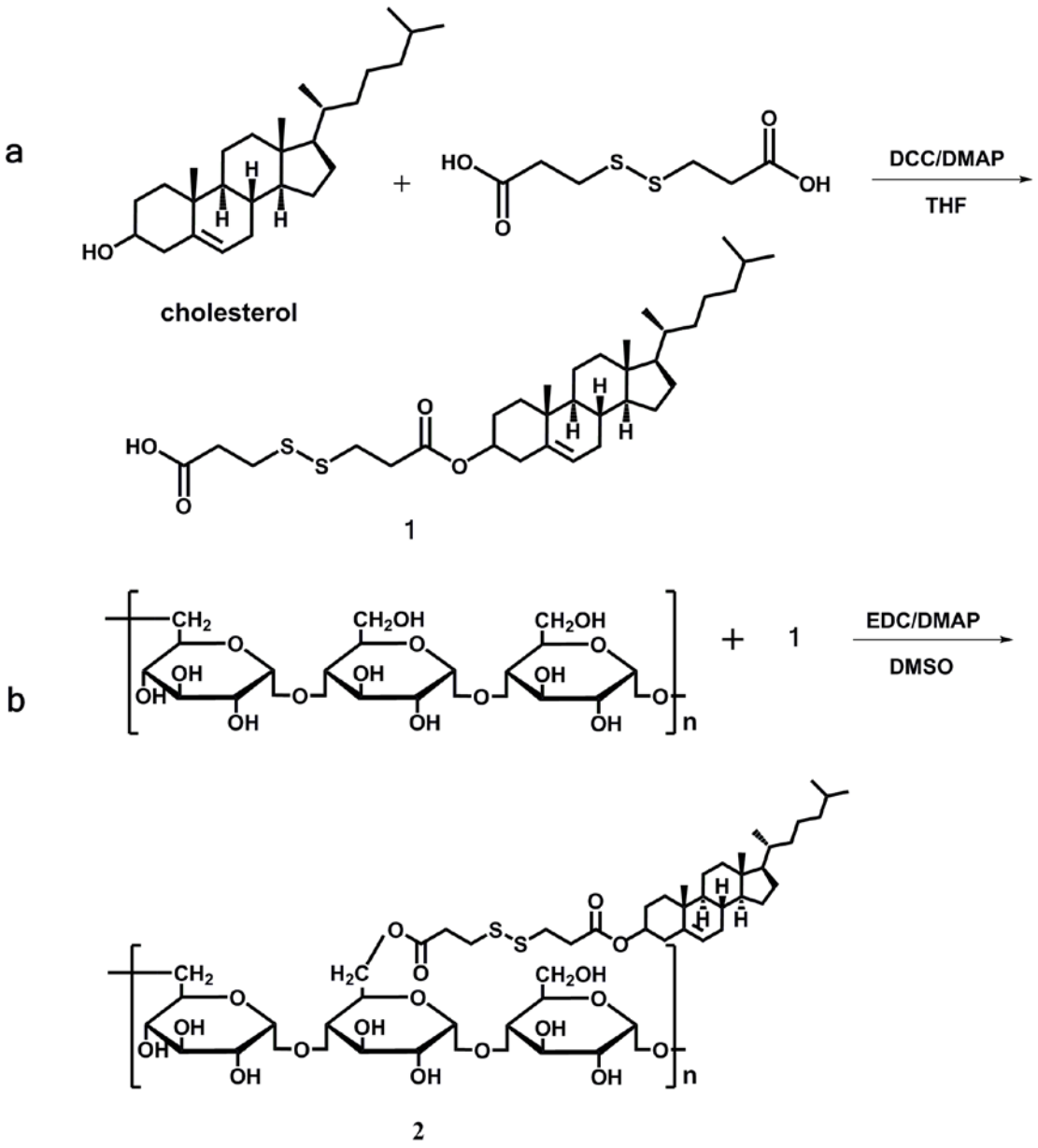

Scheme 1 Synthesis route of reducible cholesterol modified pullulan.

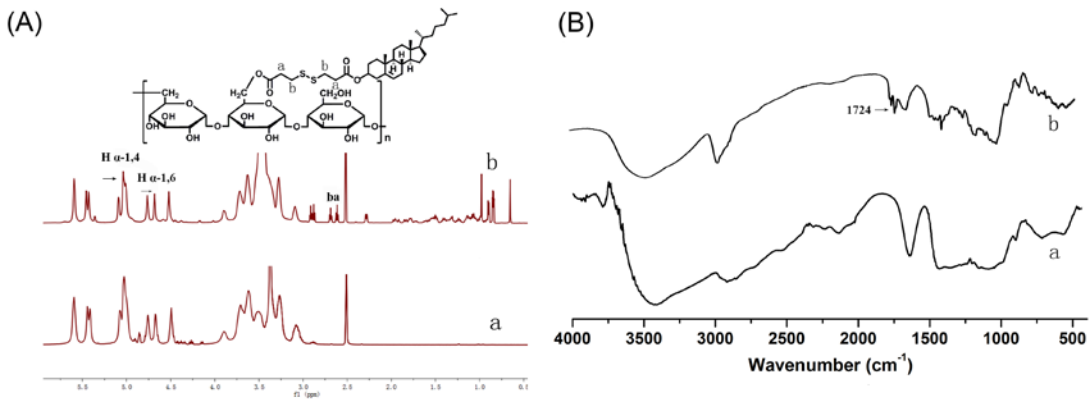

Fig.1 Representative ^{1}H-NMR (A) and FT-IR (B) spectra of pullulan (a) and reducible cholesterol modified pullulan rCHP 1 (b).

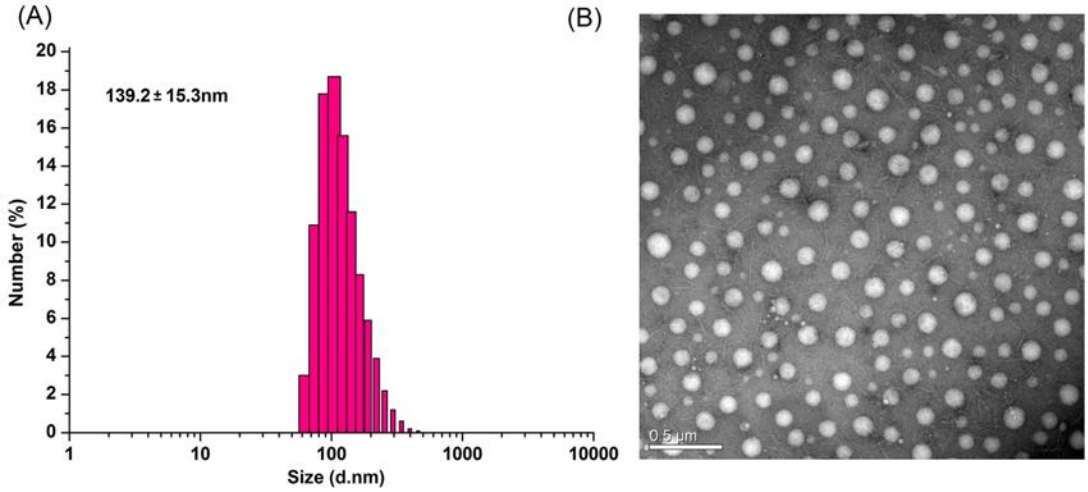

Fig.2 Representative DLS (A) and TEM (B) image of DOX-loaded nanoparticle rCHP 3c.

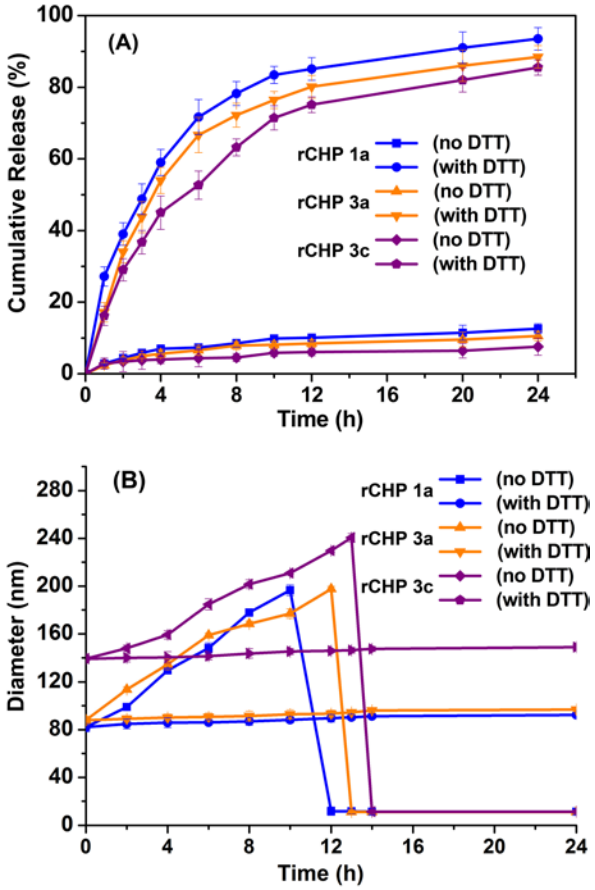

Fig.3 (A) In vitro drug releases from rCHP 1a, rCHP 3a, and rCHP 3c nanoparticles in PBS buffer solution (pH 7.4) at 37℃ without or with 10 mM DTT (n = 3). (B) Size change of rCHP 1a, rCHP 3a, and rCHP 3c nanoparticles during the drug release process (n = 3).

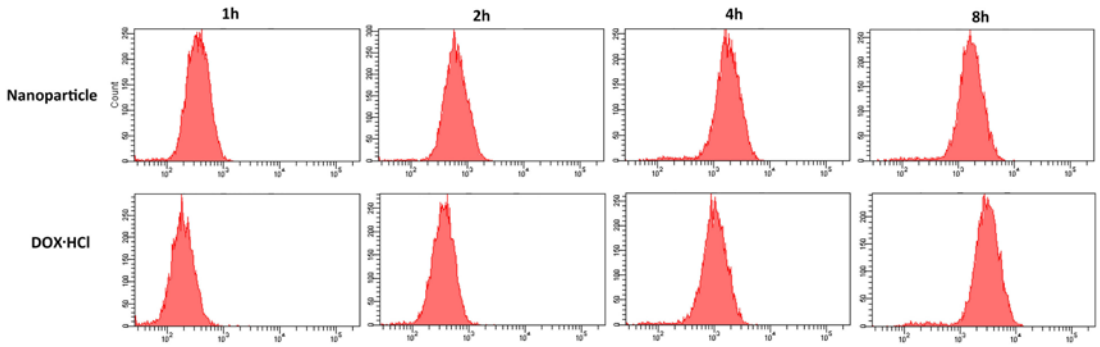

Fig.4 Flow cytometry of HepG2 cells incubated with rCHP3c nanoparticles and DOX·HCl for 1, 2, 4, 8 h (DOX concentration 1 mg/L).

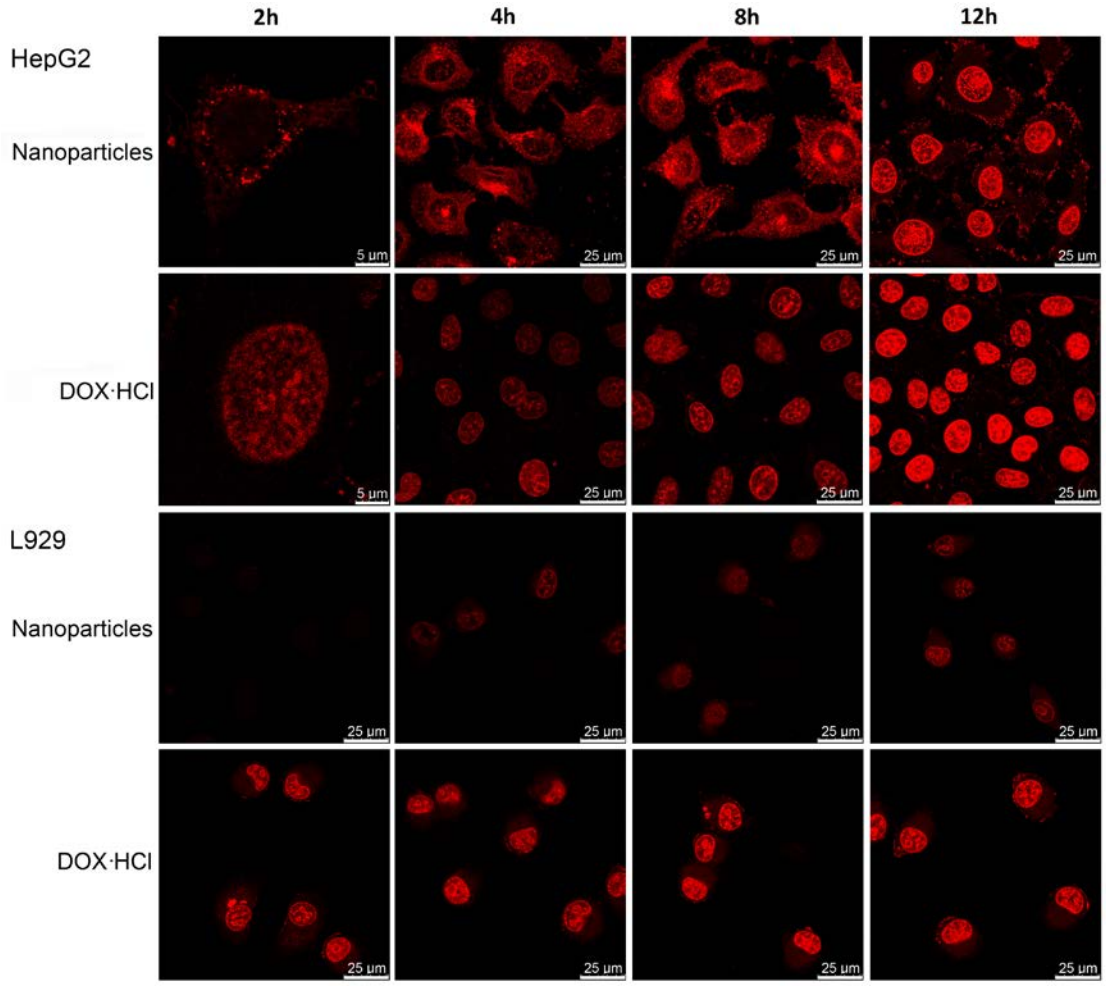

Fig.5 Confocal laser scanning microscopy images of HepG2 cells and L929 cells incubated with rCHP 3c nanoparticles and DOX·HCl at 37°C for 2, 4, 8, and 12 h (DOX concentration 5mg/L).

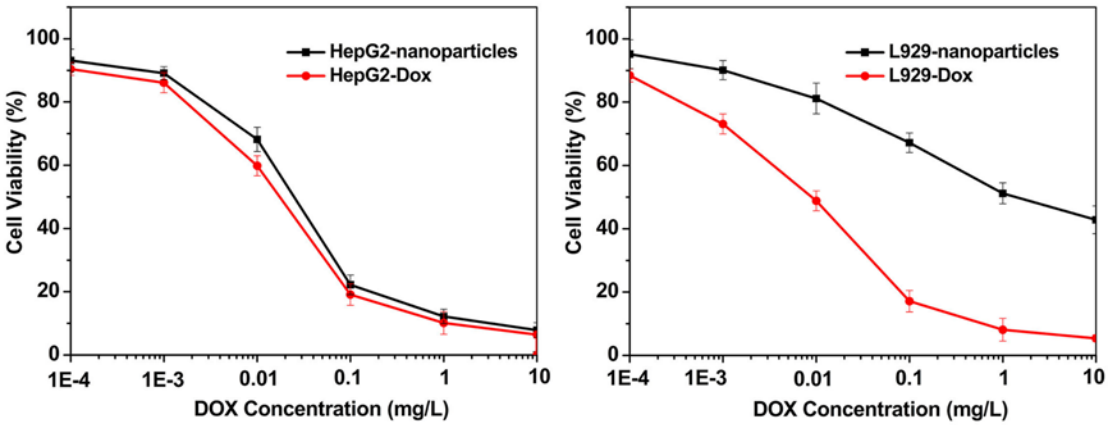

Fig.6 Cytotoxicity of rCHP 3c nanoparticles and DOX·HCl against HepG2 cells and L929 cells at various DOX concentrations.

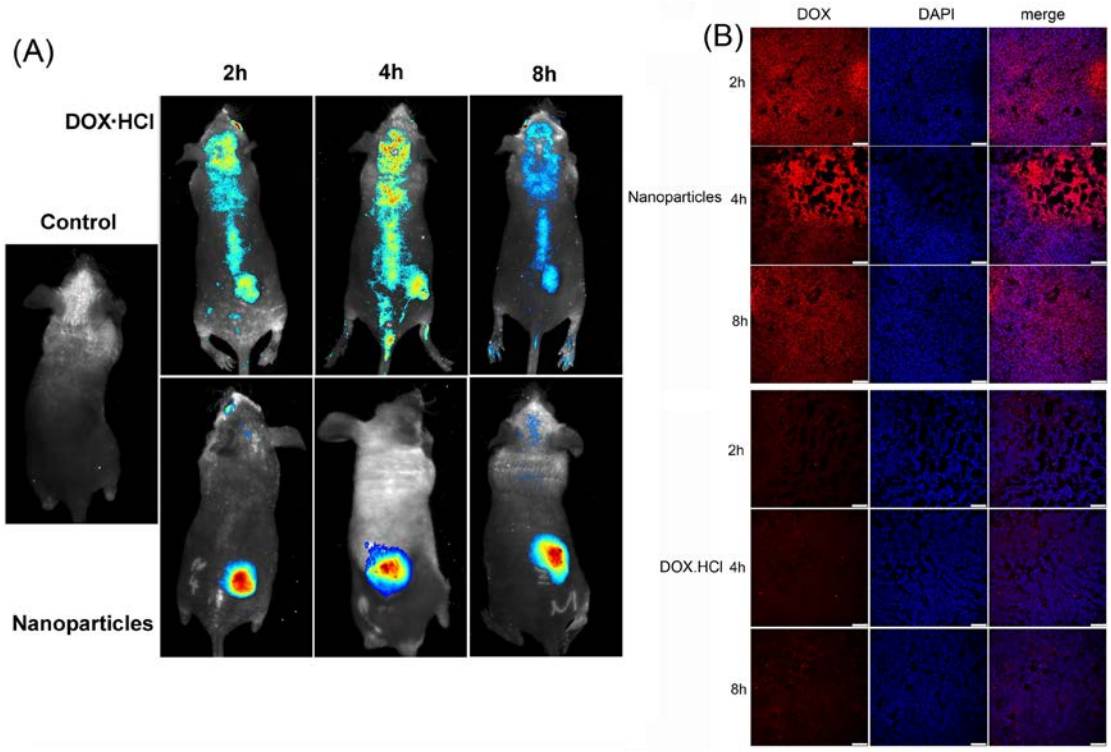

Fig.7 (A) In vivo optical fluorescence imaging of hepatoma tumor-bearing nude mice administrated with rCHP 3c nanoparticles and DOX·HCl for 2, 4, and 8 h post-injection (10 mg/kg of DOX equivalent dosage). (B) Confocal laser scanning microscopy images of tumor cryosections after injection of rCHP 3c nanoparticles and DOX·HCl for 2, 4, and 8 h. Blue fluorescence showed nuclear staining with DAPI and red fluorescence showed the location of doxorubicin. Scale bar 50 μm.

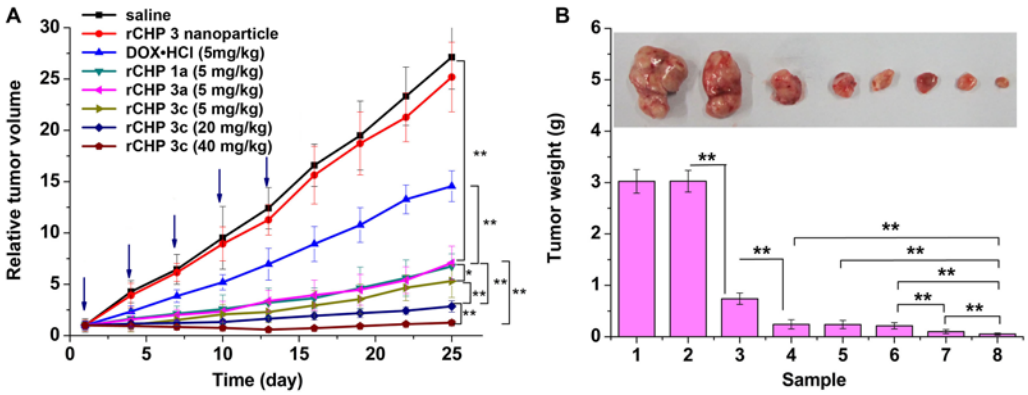

Fig.8 In vivo anticancer effect of nanoparticles. (A) Tumor volume change in the hepatoma tumor-bearing nude mice after injection of saline and various DOX formula (n = 6). (B) At the end of this experiment, tumor tissues were collected from each sacrificed animal after 25 days treatment and weighted. 1. saline; 2. rCHP 3 nanoparticle; 3. DOX·HCl (5mg/kg); 4. rCHP 1a (5 mg/kg); 5. rCHP 3a (5 mg/kg); 6. rCHP 3c (5 mg/kg); 7. rCHP 3c (20 mg/kg); 8. rCHP 3c (40 mg/kg). (n = 6).

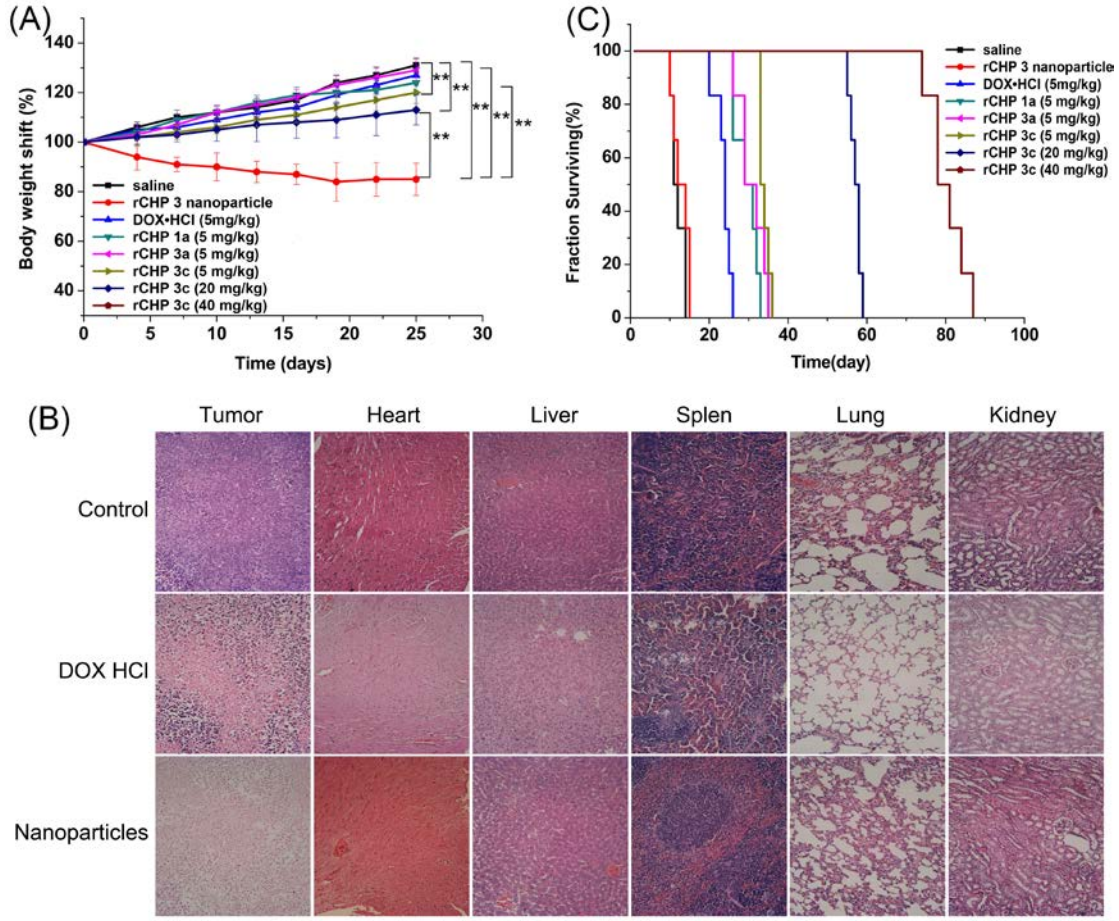

Fig.9 In vivo chemo therapy of NPs. (A) Bodyweight change of hepatoma tumor-bearing nude mice after injection of saline and various DOX formula (n = 6). (B) Histological observation for different organs of tumor-bearing nude mice administrated with DOX·HCl and rCHP 3c nanoparticles (control: PBS. tumor: ×200, heart: ×200, lung: ×200, liver: ×200, kidney: ×200). (C) Survival rates of mice bearing tumors after treatments.

Graphical abstract

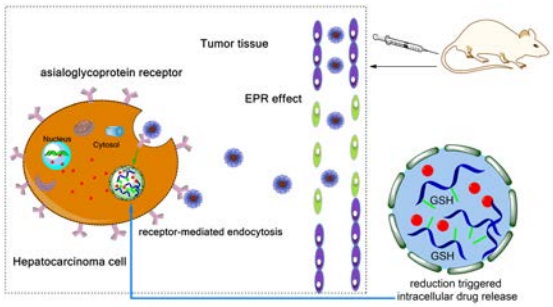

Reduction breakable nanoparticles derived from pullulan enhanced the tumor accumulation and intracellular release of DOX in hepatocellular carcinoma.